ACS APPLIED MATERIALS & INTERFACES

Research Article

www.acsami.org

High Electrochemical Performance of Monodisperse $NiCo_2O_4$ Mesoporous Microspheres as an Anode Material for Li-Ion Batteries

Jingfa Li,[†] Shenglin Xiong,*[,†] Yurong Liu,[†] Zhicheng Ju,[‡] and Yitai Qian[†,‡]

[†]Key Laboratory of the Colloid and Interface Chemistry (Shandong University), Ministry of Education, and School of Chemistry and Chemical Engineering, Shandong University, Jinan, Shandong, 250100, P. R. China

[‡]Hefei National Laboratory for Physical Science at Microscale and Department of Chemistry, University of Science and Technology of China, Hefei, Anhui, 230026, P. R. China

Supporting Information

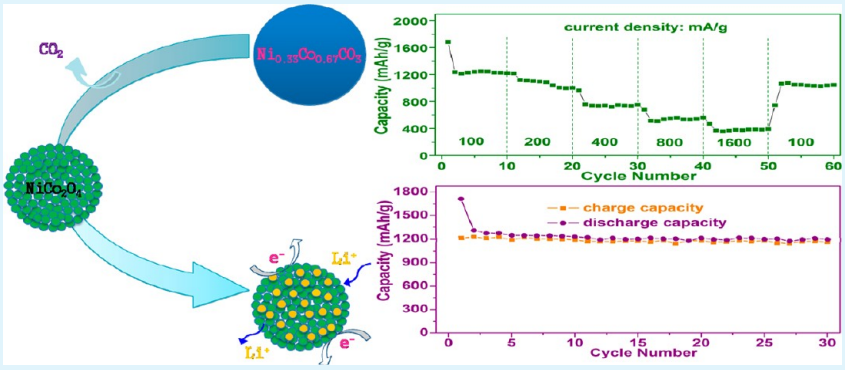

ABSTRACT: Binary metal oxides have been regarded as ideal and potential anode materials, which can ameliorate and offset the electrochemical performance of the single metal oxides, such as reversible capacity, structural stability and electronic conductivity. In this work, monodisperse $NiCo_2O_4$ mesoporous microspheres are fabricated by a facile solvothermal method followed by pyrolysis of the $Ni_{0.33}Co_{0.67}CO_3$ precursor. The Brunauer–Emmett–Teller (BET) surface area of $NiCo_2O_4$ mesoporous microspheres is determined to be about 40.58 $m^2\ g^{-1}$ with dominant pore diameter of 14.5 nm and narrow size distribution of 10–20 nm. Our as-prepared $NiCo_2O_4$ products were evaluated as the anode material for the lithium-ion-battery (LIB) application. It is demonstrated that the special structural features of the $NiCo_2O_4$ microspheres including uniformity of the surface texture, the integrity and porosity exert significant effect on the electrochemical performances. The discharge capacity of $NiCo_2O_4$ microspheres could reach 1198 mA h g^{-1} after 30 discharge–charge cycles at a current density of 200 mA g^{-1}. More importantly, when the current density increased to 800 mA·g^{-1}, it can render reversible capacity of 705 mA h g^{-1} even after 500 cycles, indicating its potential applications for next-generation high power lithium ion batteries (LIBs). The superior battery performance is mainly attributed to the unique micro/nanostructure composed of interconnected $NiCo_2O_4$ nanocrystals, which provides good electrolyte diffusion and large electrode–electrolyte contact area, and meanwhile reduces volume change during charge/discharge process. The strategy is simple but very effective, and because of its versatility, it could be extended to other high-capacity metal oxide anode materials for LIBs.

KEYWORDS: *mesoporous structures, complex metal oxides, spinel structure, lithium-ion battery*

1. INTRODUCTION

Over the past few years, the development of transition metal oxide materials with different morphologies at micro- to nanoscales are noted to be one of the substantive challenges in materials science and technology because of the potential application in the fields of ion exchange,[1] catalysis processes,[2] lithium-ion batteries (LIBs),[3] and supercapacitors.[4] Moreover, the exploration of electrode candidates in prospect has been carried out by generations of efforts. Transition metal oxides with nanostructural characteristic attracted broad attention because of their advantages of high surface-to-volume ratio and short path length for Li-ion diffusion in comparison with their bulk counterparts. In particular, such structures as Co_3O_4, Fe_2O_3, and MnO_2[5−8] have been among the most widely investigated alternative anode materials for use in LIBs over the past decade because of their high specific capacity (500 to 1000 mA h g^{-1}), compared with the 372 mA h g^{-1} for conventional graphite. Comparative study of the several transition metal oxides revealed that the best anodic performance was exhibited by cobalt oxides. Tarascon's group[5] have reported capacity values as high as ∼900 mA h g^{-1} and remaining stable up to 25 cycles for cubic spinel Co_3O_4. Recently Kang et al. have also

Received: November 8, 2012
Accepted: January 8, 2013
Published: January 16, 2013

reported a capacity of 700 mA h g^{-1} and stable up to 100 cycles with Co_3O_4.[6] However, due to the fact that cobalt is toxic and expensive, serious efforts are made toward replacing Co_3O_4 partially by eco-friendly and cheaper alternative metals. To this end, preliminary anodic properties have been reported on $NiCo_2O_4$,[9] $ZnCo_2O_4$,[10] $CuCo_2O_4$,[11] and $MnCo_2O_4$,[12] which are all isostructural to Co_3O_4.

Among various binary metal oxides above, $NiCo_2O_4$ is considered as a very promising electrode material for supercapacitor because of its good electronic conductivity, low diffusion resistance to protons/cations, and easy electrolyte penetration.[13−15] Obviously, these prominent features are in favor of the development of high-performance electrode materials. For instance, $NiCo_2O_4$ nanowires have been fabricated via a polymer/surfactant-assisted solution method, indicating higher capacitance and better cycling stability.[16,17] More recently, Lou and co-workers have synthesized $NiCo_2O_4$ nanosheets/nanowires on conductive substrates for achieving excellent cycling performance and rate capability.[18,19] However, to the best of our knowledge, it is quite surprising to note that there have been few studies on the preparation of $NiCo_2O_4$-based micro/nanostructured electrode materials for lithium-ion batteries,[9] although some documents have already been reported about the application for the supercapacitor of $NiCo_2O_4$.

In addition, mesoporous materials exhibit excellent electrochemical performances because of their high specific surface areas that can promote the interface contact between electrode and electrolyte, and the mesopores that allow the liquid electrolyte to easily diffuse into the electrode materials, leading to a high flux of lithium ions across the interface and providing space for volume expansion during the discharge and charge processes.[20,21] In general terms, mesoporous materials are synthesized with the template-directed methods by adopting the hard templates such as mesoporous silica or carbon[22,23] and the soft templates such as surfactants or long-chain polymers.[24,25] However, some obstacles such as the fussy multistep procedures and the residual templates in the resultant samples always harass these methods.

Herein, we report a simple template-free solvothermal route followed by the thermal posttreatment of precursor for the synthesis of monodisperse $NiCo_2O_4$ mesoporous microspheres, which displayed superior battery performance. The whole experimental flowchart is schematically illustrated in Figure 1. Briefly, in step I, monodisperse $Ni_{0.33}Co_{0.67}CO_3$ microspheres are fabricated by a facile solvothermal process without any template or surfactant. In step II, the $Ni_{0.33}Co_{0.67}CO_3$ microspheres are calcined under air atmosphere to transform into the mesoporous $NiCo_2O_4$ microspheres by the release of CO_2 gas. When evaluated as anode materials for LIBs, as shown in step III, the Li^+ ions can diffuse into the $NiCo_2O_4$ microspheres through these pores with short distance and little resistance, favorably enhancing the electrochemical behaviors. It is found that the as-prepared sample has a relatively high specific surface area of 40.58 m^2 g^{-1} and a narrow pore size distribution of 10−20 nm (centered at 14.5 nm), and they exhibit a high initial discharge capacity and could retain a high capacity of 705 mA h g^{-1} at a current density of 800 mA g^{-1} even after 500 charge/discharge cycles, indicating its good potential application for high power applications in LIBs.

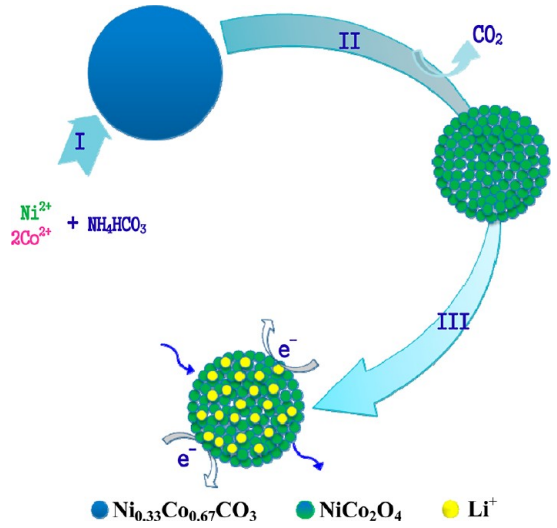

Figure 1. Schematic illustration of the formation of $NiCo_2O_4$ mesoporous microspheres and their presented electrochemical property in lithium-ion storage.

2. EXPERIMENTAL SECTION

Preparation of Monodisperse $NiCo_2O_4$ Mesoporous Microspheres. The chemicals used in our experiments were purchased from Shanghai Sinopharm Chemical Reagent Co. Ltd. and used after grounded manually for several minutes to accelerate the dissolution rate in the solvent. In a typical synthesis of $Ni_{0.33}Co_{0.67}CO_3$ precursor, for example, 1 mmol of $NiCl_2{\cdot}4H_2O$ and 2 mmol of $CoCl_2{\cdot}6H_2O$ were dissolved into 40 mL of ethylene glycol under magnetic stirring. Then, 30 mmol of NH_4HCO_3 was added to the mixture solution at room temperature. The resultant mixture was continually stirred for 30 min and then transferred into a Teflon lined stainless-steel autoclave (capacity of 60 mL). The autoclave was sealed and maintained at 200 °C for 20 h in an electron oven. The product of $Ni_{0.33}Co_{0.67}CO_3$ precursor was collected and washed with distilled water and absolute alcohol several times, followed by vacuum-drying at 60 °C. Then, after calcining the collected precursors at 450 °C for 10 h in air, black composite metal oxides $NiCo_2O_4$ were obtained. The sample was then ready for further characterization.

Instrumentation and Sample Analysis. The crystallographic information of the prepared samples was established by powder XRD (XRD, Philips X'Pert Pro Super diffractometer with Cu K_α radiation (λ = 1.54178 Å)). We have carried out the X-ray diffraction of the $NiCo_2O_4$ with a slow scan speed of 0.0039° s^{-1} in the 2θ range of 10 to 80°, which lasted 5 h for the purpose of Rietveld refinement.[26] The Rietveld refinement software used is GSAS.[27] Field-emission scanning electronic microscopy (FESEM, JSM-6700F) was employed to examine the morphologies of the products. Structural and compositional investigations by transmission electron microscopy (TEM) and high-resolution TEM (HRTEM) were carried out using JEM-2100F (JEOL) and energy dispersive spectrometer (EDS) instruments, operated with an electron kinetic energy of 200 kV. Surface analysis of the studied samples was performed using XPS (VGESCA-LABMKIIX-ray photoelectronic spectrometer). Thermogravimetric analysis (TGA-2050 (TA Corp.)) was also conducted to determine the composition of samples. The TGA measurements were carried out at a heating rate of 10 °C min^{-1} from 20 to 800 °C with an air flow-rate of 100 mL min^{-1}. The measurements of the specific surface area and the analysis of the porosity of $NiCo_2O_4$ products were performed through measuring N_2 adsorption−desorption isotherms at 77 K, using a Micrometrics ASAP 2020 M system.

Electrochemical Measurements. The electrochemical tests were performed under ambient temperature using two-electrode coin cells (size: 2032) with lithium serving as both the counter electrode and the reference electrode. The working electrode was prepared by mixing 50 wt % active material (e.g., as-prepared $NiCo_2O_4$ mesoporous

dx.doi.org/10.1021/am3026294 | ACS Appl. Mater. Interfaces 2013, 5, 981−988

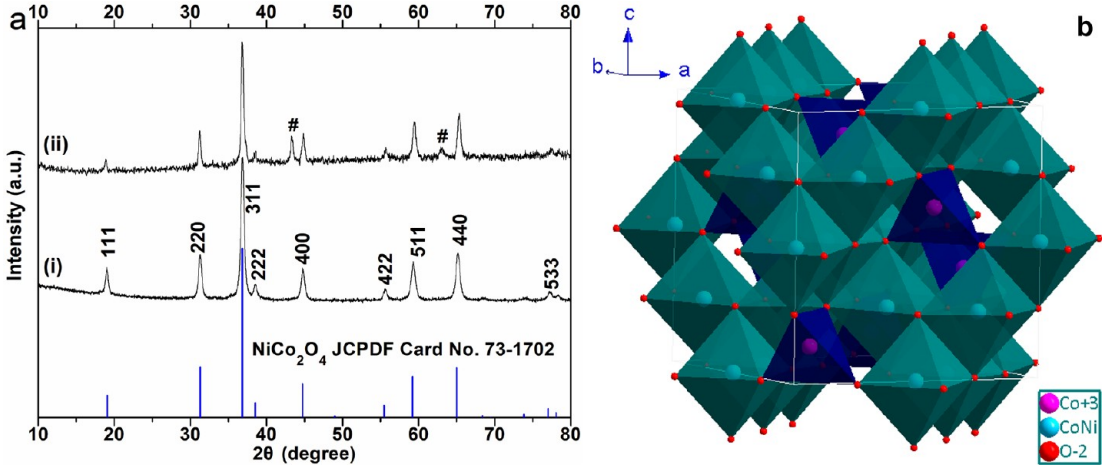

Figure 2. (a) XRD patterns of two samples obtained by calcining $Ni_{0.33}Co_{0.67}CO_3$ precursors at (i) 450 °C and (ii) 600 °C for 10 h in air. Notes: (#) cubic NiO (JCPDS No. 65−2901). (b) Schematic representation of $NiCo_2O_4$ cubic spinel (ICSD No. 02241).

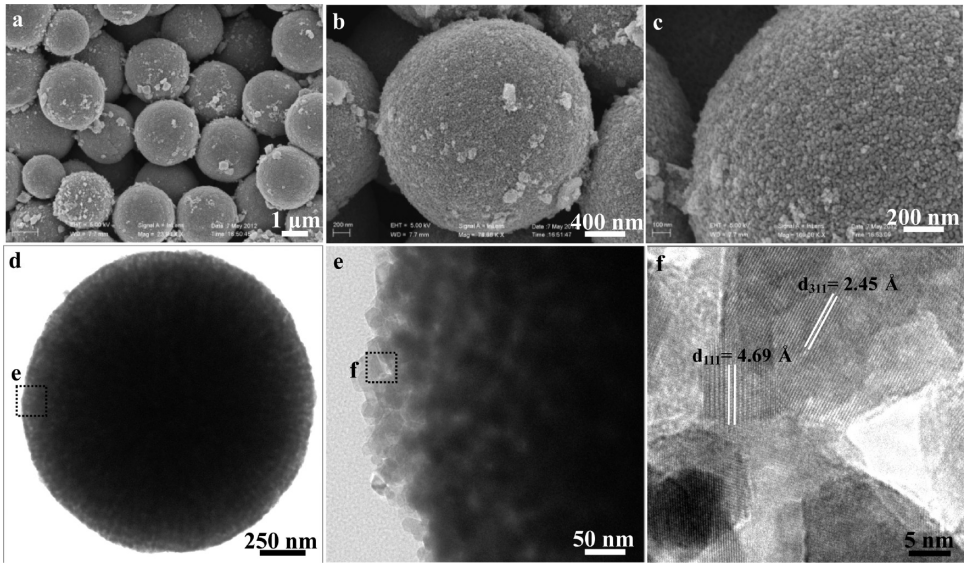

Figure 3. Characterization of $NiCo_2O_4$ mesoporous microspheres: (a−c) SEM images; (d, e) TEM images; (f) high-resolution TEM images.

microspheres), 30 wt % conductivity agent (acetylene black, Super P), and 20 wt % binder (polyvinylidene difluoride, PVDF, Aldrich) onto a copper foil substrate. The electrodes were dried at 120 °C in a vacuum oven for 12 h before assembling. The electrolyte used in the cells was 1.00 M $LiPF_6$ in a 50:50 (w/w) mixture of ethylene carbonate (EC) and diethyl carbonate (DEC). The cell assembly was carried out in an argon-filled glovebox with both the moisture and the oxygen content below 1 ppm. Galvanostatic charge/discharge was conducted using a battery tester (LAND-CT2001A) with a voltage window of 0.01−3.0 V at a setting current rate. The cyclic voltammetry (CV) test was carried out in the potential window of 0.01 to 3.0 V by an electrochemical workstation (CHI 660). Electrochemical impedance spectroscopy (EIS) was carried out on an electrochemical workstation (Materials Mates 510, Italia) in the frequency range from 0.1 MHz to 0.01 Hz.

3. RESULT AND DISCUSSION

Monodisperse carbonate microspheres are first prepared by ammonium hydrogen carbonate-assisted solvothermal process. The X-ray diffraction (XRD) peaks (see the Supporting Information (SI), Figure S1) indicate the formation of calcite $Ni_{0.33}Co_{0.67}CO_3$. Field-emission scanning electron microscope (FESEM) observation reveals that the $Ni_{0.33}Co_{0.67}CO_3$ precursors are composed of uniform and monodisperse microspheres with the size of 2.5−3.0 μm (see the Supporting Information, Figure S2). Thermogravimetric analysis (TGA, Figure S3) reveals that thermal decomposition of the $Ni_{0.33}Co_{0.67}CO_3$ into $NiCo_2O_4$ in air is completed at 450 °C, and the calculated value of weight loss is very close to the theoretical value (32.81% vs 32.54%). Thus, a temperature of 450 °C is chosen as the calcination temperature for the synthesis of $NiCo_2O_4$ phase. As expected, the $Ni_{0.33}Co_{0.67}CO_3$ is transformed into $NiCo_2O_4$ after annealing at 450 °C in air. XRD characterization in Figure 2a (sample (i)) indicates that the product can be indexed as face-centered-cubic (fcc) $NiCo_2O_4$ (a_0 = 8.269 Å; space group *Fd*3*m* (227), JCPDS No. 73−1702). The Rietveld refinement of the XRD data confirms the $NiCo_2O_4$ phase without other imputy like NiO (see the Supporting Information, Figure S4). It is generally believed to adopt a spinel-related structure in which nickel occupies the octahedral sites and cobalt is distributed over both octahedral and tetrahedral sites,[28,29] as illustrated in Figure 2b. It is observed from the TGA result that the higher calcination temperature (from 500 to 800 °C) can lead to the

dx.doi.org/10.1021/am3026294 | ACS Appl. Mater. Interfaces 2013, 5, 981−988

decomposition of $NiCo_2O_4$ sample. The XRD peaks of the sample calcined at 600 °C (Figure 2a, sample (ii)) indicated the coexisting with cubic NiO (JCPDS No. 65−2901), which is also observed by Lin[13] and Chen et al.[30]

The morphology and microstructure of the as-synthesized $NiCo_2O_4$ mesoporous microspheres are examined with scanning electron microscopy (SEM) and transmission electron microscopy (TEM). From the SEM image shown in Figure 3a, we find that the overall morphology of $NiCo_2O_4$ microspheres is very similar to $Ni_{0.33}Co_{0.67}CO_3$ precursors. As shown in panels b and c in Figure 3, each microsphere is composed of numerous primary particles with size of tens of nanometers, which results from the release of CO_2 gas during the decomposition of $Ni_{0.33}Co_{0.67}CO_3$. The porosity of the $NiCo_2O_4$ microspheres is clearly revealed by defined contrast of the microsphere perimeter in Figure 3d, although it is difficult to observe the contrast in the center due to the larger size of the microsphere. Figure 3e shows a TEM image displaying a selected area at the edge of single sphere. From the relative light contrast, it can be clearly observed the existence of pores. A representative high-resolution TEM image is shown in Figure 3f, the measured interplanar distance is 4.69 and 2.45 Å, which matches well to the (111) and (311) planes of spinel $NiCo_2O_4$, respectively. The chemical compositions of the products have been analyzed by energy-dispersive X-ray spectroscopy (EDX) (SI, Figure S5), which indicates an atomic Ni/Co ratio of 1:2.

Here we also confirm the porosity by N_2 sorption measurements. As shown in Figure 4, the N_2 adsorption−desorption isotherm is characteristic of type IV with a type H2 hysteresis loop observed in the range 0.8−1.0 p/p_0, which might appear to be a unique characteristic of mesopores (the hollow interstice). The inset in the Figure 4 shows the corresponding pore size distribution calculated by the Barrett−Joyner−Halenda (BJH) method from the desorption branch, indicating a narrow pore size distribution (10−20 nm) centered at around 14.5 nm. Thus, it can be concluded that the sample is characteristic of mesoporous materials.[31] According to the investigative results, the $NiCo_2O_4$ microspheres give rise to a relatively high Brunauer−Emmett−Teller (BET) specific surface area of 40.58 $m^2\ g^{-1}$ and a pore volume of 0.217 $cm^3\ g^{-1}$. Considering its mesoporous structure favoring the diffusion of Li^+ ions and electrode−electrolyte contacts during the electrochemical reaction, the $NiCo_2O_4$ microspheres are expected to improve the electrochemical performance.

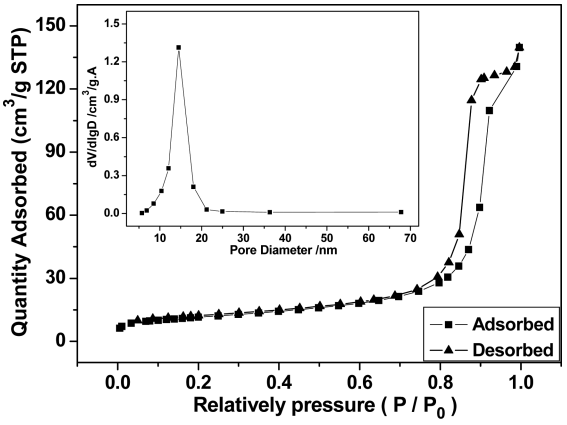

Figure 4. Nitrogen adsorption−desorption isotherm and the corresponding pore size distribution (inset) of $NiCo_2O_4$ mesoporous microspheres.

The more detailed elemental composition and oxidation state of the as-prepared $NiCo_2O_4$ are further characterized by X-ray photoelectron (XPS) measurements and the corresponding results are presented in Figure 5. The survey spectrum (Figure 5a) indicates the presence of Ni, Co and O as well as C from the reference and the absence of other impurities. By using a Gaussian fitting method, the Ni 2p emission spectrum (Figure 5b) was best fitted with two spin−orbit doublets, characteristic of Ni^{2+} and Ni^{3+}, and two shakeup satellite (identified as "Sat."). The Co 2p spectrum (Figure 5c) was best fitted considering two spin−orbit doublets characteristic of Co^{2+} and Co^{3+} and two couple of shakeup satellites. These results show that the chemical composition of $NiCo_2O_4$ mesoporous microspheres contain Co^{2+}, Co^{3+}, Ni^{2+}, and Ni^{3+}, which are in good agreement with the results in the literature for $NiCo_2O_4$.[32−34] The high-resolution spectrum for the O 1s region (Figure 5d) shows three oxygen contributions. Specifically, the peak at 529.6 eV is typical of metal−oxygen bonds.[34,35] The peak sitting at 531.0 eV is usually associated with defects, contaminants, and a number of surface species including hydroxyls, chemisorbed oxygen, under-coordinated lattice oxygen, or species intrinsic to the surface of the spinel.[36,37] The peaks at ∼532.9 eV can be attributed to multiplicity of physi- and chemi-sorbed water at or near the surface.[34,35] Thus, the electron couples of Ni^{3+}/Ni^{2+} and Co^{3+}/Co^{2+} (the ratios are shown in Table S1 in the Supporting Information based on the area of deconvolved peaks) are coexisting in the spinel $NiCo_2O_4$ structures, where the total atomic ratio of Ni and Co elements is ca. 0.9:2.1, corresponding to the result (1:2) indicated by energy-dispersive X-ray spectroscopy (EDX).

With the combined properties of porous inside architecture and high surface area, the as-prepared $NiCo_2O_4$ mesoporous microspheres may display promising applications in a variety of fields. To evaluate whether the porous structure would be applicable in lithium-ion batteries, the as-prepared products were used as anode materials in tests. Figure 6 shows the first four cyclic voltammetry (CV) curves of the electrode made from the porous $NiCo_2O_4$ microspheres at a scan rate of 0.1 mV s^{-1}. The voltammogram for the first cycle is substantially different from those of the subsequent ones. In the first cathodic sweep, the intense peak at 0.85 V can be ascribed to the reduction of Ni^{2+} and Co^{3+} to metallic Ni and Co, respectively. The main reduction peak shifts to a higher potential at 1.0 V in the subsequent cycles, which might be originate from the pulverization of the $NiCo_2O_4$. The following anodic sweep is characterized by two oxidation peaks at ∼1.6 V and ∼2.1 V, which can be attributed to the oxidation of Ni^0 to Ni^{2+} and Co^0 to Co^{3+}. On the basis of the cyclic voltammograms, together with the storage mechanisms of NiO, Co_3O_4, and CoO that have been previously reported,[38,39] the entire electrochemical process can be classified as follows

$$NiCo_2O_4 + 8Li^+ + 8e^- \rightarrow Ni + 2Co + 4Li_2O \quad (1)$$

$$Ni + Li_2O \leftrightarrow NiO + 2Li^+ + 2e^- \quad (2)$$

$$Co + Li_2O \leftrightarrow CoO + 2Li^+ + 2e^- \quad (3)$$

$$CoO + 1/3Li_2O \leftrightarrow 1/3Co_3O_4 + 2/3Li^+ + 2/3e^- \quad (4)$$

When the $NiCo_2O_4$ microspheres are electrochemically discharged with lithium metal, crystal structure destruction occurs,

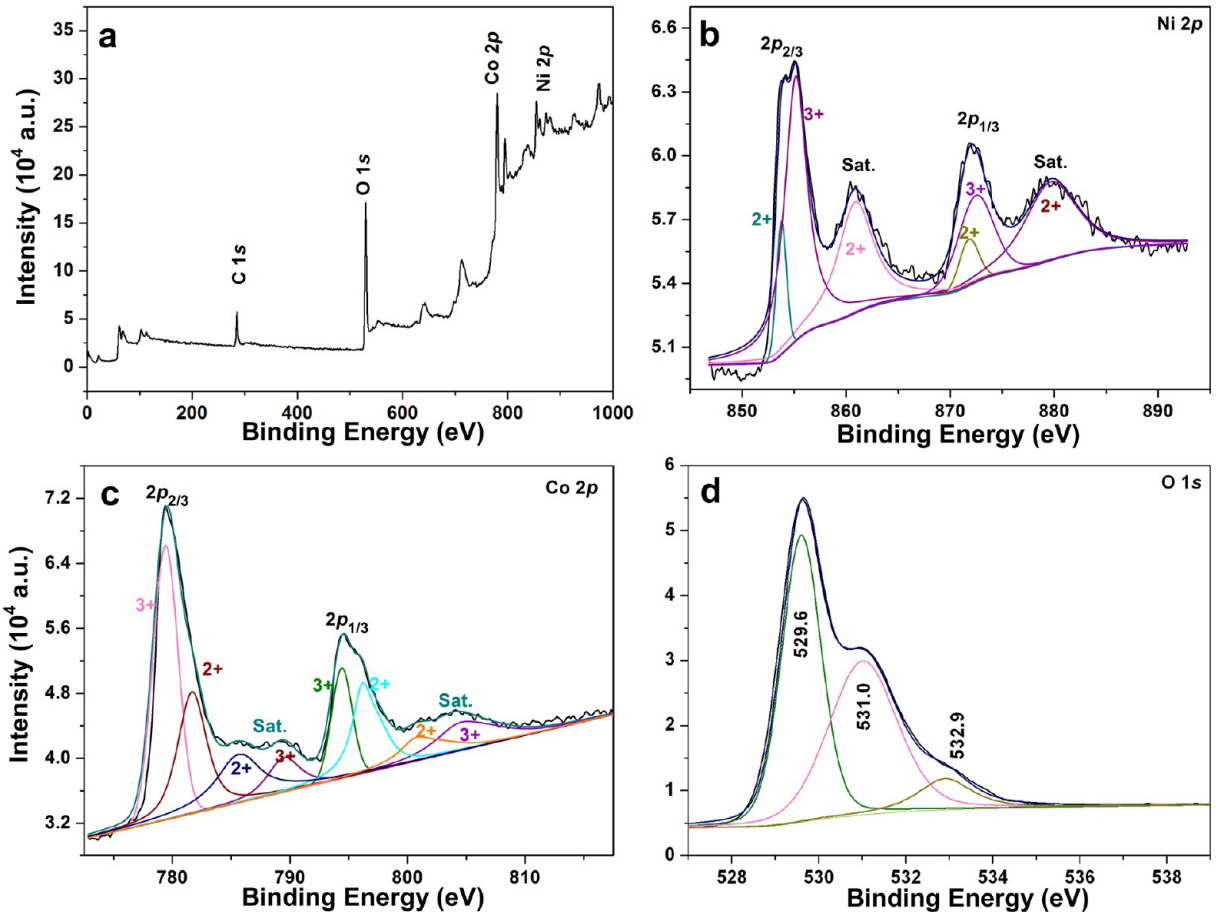

Figure 5. XPS spectra of (a) survey spectrum, (b) Ni 2p, (c) Co 2p, and (d) O 1s for $NiCo_2O_4$ mesoporous microspheres.

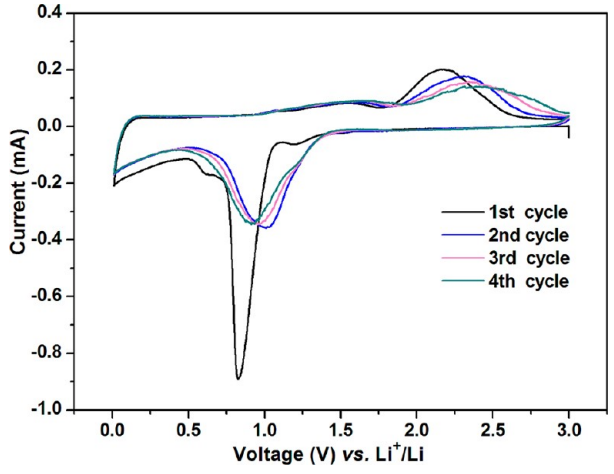

Figure 6. First four cycles of CVs for the $NiCo_2O_4$ mesoporous microspheres at a scan rate of 0.1 mV s^{-1} in the voltage of 0.01−3.0 V.

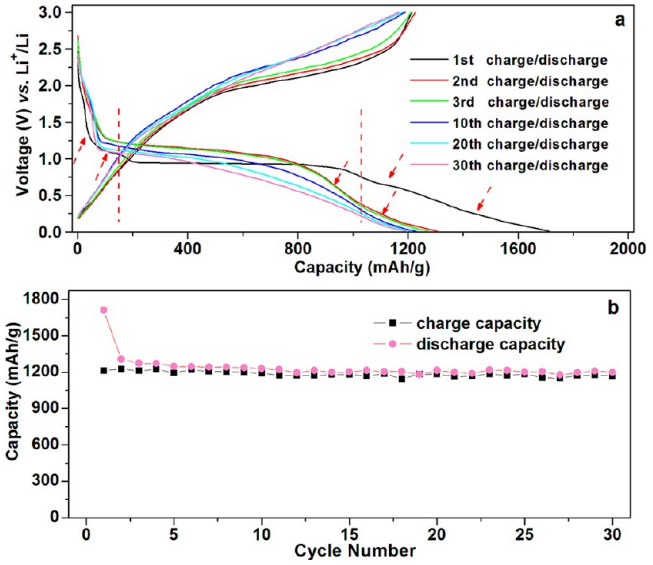

Figure 7. Electrochemical performance of $NiCo_2O_4$ electrode: (a) discharge/charge profiles for the selected cycles and (b) cycle performance at a current of 200 mA g^{-1}.

followed by the formation of nanosized Ni, Co, and Li_2O, as shown in eq 1. Then, the consequent electrochemical process may be the combined reaction, based on the NiO (eq 2) and Co_3O_4 (eq 3 and eq 4), respectively. The electrochemical process of individual NiO and Co_3O_4 components as the LIBs anode, have been elucidated clearly in many papers.

Figure 7a shows the selected charge and discharge cycle profiles of the electrode at a current density of 200 mA g^{-1} in the range of 0.01−3.0 V. It can be seen that all these discharge curves exhibit one plateau between 0.9 and 1.1 V. Among them, the plateau of the first discharge curve is slightly lower than others, which is associated with the irreversible reaction of $NiCo_2O_4$ and Li^+ as eq 1, in consistence with the above CV detection results. The first discharge capacity reached about 1712 mA h g^{-1} (equivalent to ~15.3 mol Li per mole of

dx.doi.org/10.1021/am3026294 | ACS Appl. Mater. Interfaces 2013, 5, 981−988

$NiCo_2O_4$), overnumbering the theoretically delivered 8 mol Li indicated in eq 1. The residue extra capacities of about 814 mA h g^{-1}, corresponding to the two slope ranges marked by the red arrows, are ascribed to the formation of solid electrolyte interface (SEI) film[40] and organic polymeric/gel-like layer by electrolyte decomposition.[41] Obviously, at the 0.9 V potential plateau, it delivers the majority of capacity (about 880 mA h g^{-1}, the range between the two vertical dotted lines), originating from the reduction reaction of eq 1. It can be seen that the initial specific charge capacity is about 1214 mA h g^{-1} (~10.9 mol Li), showing a capacity loss of 498 mA h g^{-1} and a charging retention of 70.9%. Besides the irreversibility of eq 1, the large irreversible capacity and low Coulombic efficiency for the first cycling is also attributed to the formation of solid electrolyte interface (SEI) film and some undecomposed Li_2O phase.[40] Figure 7b displays the corresponding discharge−charge cycling performance of the $NiCo_2O_4$/Li cell. We can observe that it had a high initial discharge capacity followed with a fast decay, however, retained a stable value of 1198 mA h g^{-1} from second to 30th discharge−charge cycle. At the same time, the corresponding specific charge capacities always keep as high as 1167 mA h g^{-1} (~10.5 mol Li), much larger than the calculated value of 7.33 mol Li based on eqs 1−4. The interfacial storage originated from the unique $NiCo_2O_4$ porous structure is considered to be responsible for the high extra capacity. As Maier et al. reported,[42] the interfacial storage is mainly from the reversible formation/dissolution of organic polymeric/gel-like layer by electrolyte decomposition, which could deliver an extra capacity through a so-called "pseudo-capacitive behavior". The mesopores with a small pore size (~14.5 nm) and the resulting large surface area of $NiCo_2O_4$ dramatically promote the surface Li storage capacities, and thus lead to an obvious sloped region during the discharge process as pointed by the right red dotted arrows in Figure 7a. With respect to capacity and cyclability, the striking improvement has been achieved by comparison with the previous work on $NiCo_2O_4$ as the anode material, wherein only 884 mA h g^{-1} was obtained even at the low current of 89 mA g^{-1}.[9]

To better understand the electrochemical behavior of the $NiCo_2O_4$ mesoporous microspheres, we also investigated its rate performance as shown in Figure 8a. The $NiCo_2O_4$ electrode was cycled at various current densities (100−1600 mA g^{-1}). The cell shows good rate capability with average discharge capacity of 1260, 1003, 753, 556, and 393 mA h g^{-1}, when the current density increased stepwise to 100, 200, 400, 800, and 1600 mA g^{-1}, respectively. Upon altering the current density back to 100 mA g^{-1}, an average discharge capacity as high as 1046 mA h g^{-1} could be recovered. This demonstrates that the $NiCo_2O_4$ mesoporous structure has great potential as high-rate anode materials in lithium-ion batteries. Considering that a high current density is very significant for practical batteries when fast discharge/charge is required, we further evaluated the $NiCo_2O_4$ electrode at a relatively high current density of 800 mA g^{-1}. As shown in Figure 8b, the discharge capacity decreased from the initial discharge capacity of 1144 mA h g^{-1} rapidly to 730 mA h g^{-1} after 50 cycles. Then it slowly reduced to 601 mA h g^{-1} after another 70 cycles. After that, the capacities of the $NiCo_2O_4$ electrode increased gradually and stabilized at 705 mA h g^{-1} after 500 cycles with a Coulombic efficiency of around 95−98%. Similar results were also observed by our previous reports on $ZnFe_2O_4$ nano-octahedrons[43] at 1000 mA g^{-1} and $Mn_{1.5}Co_{1.5}O_4$ core−shell microspheres[44] at 400 mA g^{-1}. The main reason is that the high

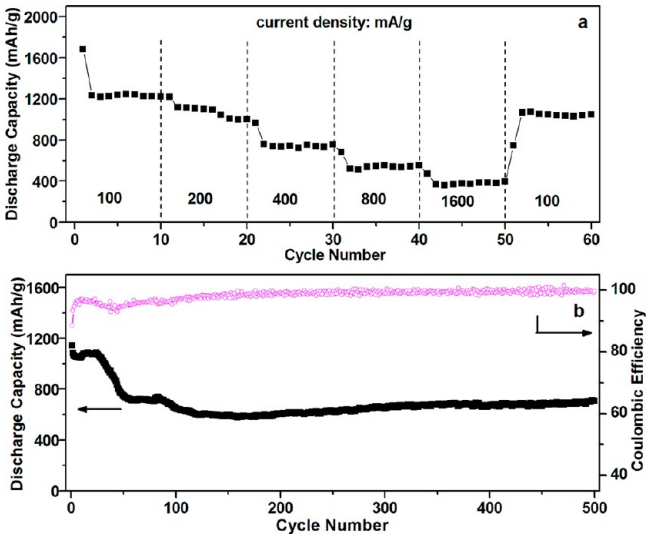

Figure 8. (a) Rate capability test for the $NiCo_2O_4$ electrode at various current densities (100−1600 mA g^{-1}). (b) Cycle performance and Coulombic efficiency for $NiCo_2O_4$ electrode at the current density of 800 mA g^{-1}.

discharge/charge current density might induce drastic structure reorganization accompanied by decomposition and reformation of the electrolyte.

To further understand the superior electrochemical performance of $NiCo_2O_4$ mesoporous microspheres as anode material, the AC impedance of $NiCo_2O_4$/Li cells in the fully discharged states at 800 mA g^{-1} after certain cycles (5th, 10th, 20th, 30th, 50th and 500th) are performed (Figure 9). The Nyquist plots

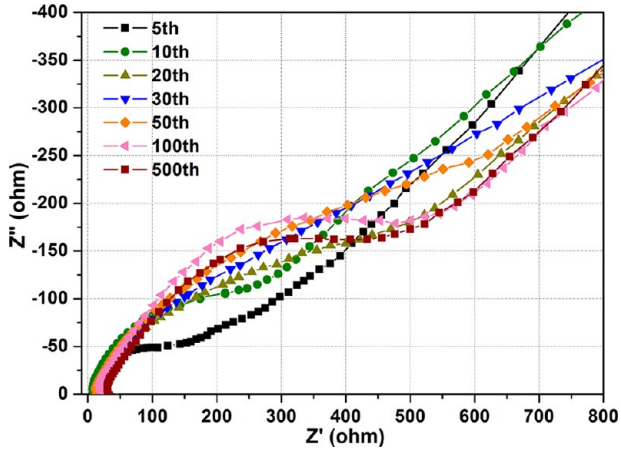

Figure 9. Nyquist plots of the cell assembled by monodisperse $NiCo_2O_4$ mesoporous microspheres after certain cycles at 800 mA g^{-1} in fully charged state in the frequency range from 0.1 MHz to 0.01 Hz.

are similar to each other in the shape, with a depressed semicircle in the high and medium frequency ranges and a straight line in the low frequency. The semicircle in the middle frequency range indicates the charge-transfer resistance (R_{ct}), relating to charge transfer through the electrode/electrolyte interface. The inclined line in the low-frequency region represents the Warburg impedance (Z_w), which is related to solid-state diffusion of Li^+ in the electrode materials.[45] As one can observe, from 5 to 50 cycles, there are obvious increases of R_{ct} estimated from the depressed semicircles. Then, the

dx.doi.org/10.1021/am3026294 | ACS Appl. Mater. Interfaces 2013, 5, 981−988

resistances gradually increase from 50 to 100 cycles. After cycled 500 times, the value of the Rct decrease slightly compared with the 100th cycled state. This impedance evolution can well match the electrochemical performance with the reversible specific capacity first decreasing from the initial discharge capacity of 1144 mA h g^{-1} rapidly to 730 mA h g^{-1} then slowly reducing to 601 mA h g^{-1} and finally stabilizing at 705 mA h g^{-1} after 500 cycles (Figure 8b).

The unique porous microspheres should contribute to the good electrochemical performances of the as-synthesized $NiCo_2O_4$ microspheres. On the one hand, the existence of pores in the $NiCo_2O_4$ favorably shortens the transport pathway for Li^+ diffusion and increases electrode−electrolyte contact area for more Li^+ migration across the interface, thus leading to the high specific capacity and superior rate capability. On the other hand, the uniformity and integrity of the microsphere composed of interconnected $NiCo_2O_4$ nanocrystals are beneficial to relieve the strain induced by the volume change and during the long-term discharge/charge cycling, hence improving cyclability. However, the intrinsic high voltage plateau of such oxides may limit the practical application in battery industry. To overcome the limitation and avoid the drawback, the nanostructured hybrid electrode materials[46] and doping with other metal cations are preferred and more detailed and further investigation is under the way.

4. CONCLUSION

In conclusion, we have devised a facile ammonium hydrogen carbonate-assisted solvothermal route to prepare $Ni_{0.33}Co_{0.67}CO_3$ microspheres. Using this solid precursor, monodisperse $NiCo_2O_4$ mesoporous microspheres have been successfully fabricated via direct thermal decomposition in laboratory air at 450 °C. The microspheres comprised numerous pores with an average size of 14.5 nm and a narrow size distribution of 10−20 nm. Such a unique porous structure not only favors the fast Li^+ transport but also accommodates the volume expansion/contraction during discharge/charge process. When used as an anode material for LIBs, the as-prepared monodisperse $NiCo_2O_4$ mesoporous microspheres show a high specific discharge capacity, superior rate capability, and excellent cycling stability. The improved electrochemical performance enables such $NiCo_2O_4$ mesoporous microspheres to be a promising anode material for next-generation, high-power lithium-ion batteries.

■ ASSOCIATED CONTENT

Supporting Information

XRD patterns, SEM images, and TGA data of the precursor, EDS analysis of the $NiCo_2O_4$ mesoporous microspheres. This material is available free of charge via the Internet at http://pubs.acs.org.

■ AUTHOR INFORMATION

Corresponding Author

*Fax: (86)-531-88363018. Tel: (86)-531-88363018. E-mail: chexsl@sdu.edu.cn.

Notes

Notes. The authors declare no competing financial interest.

■ ACKNOWLEDGMENTS

This work was supported by the National Basic Research Program of China (the 973 Project of China, 2011CB935901), the National Science Foundation of Shandong Province (ZR2012BM018), the Independent Innovation Foundations of Shandong University (2012ZD008), the National Natural Science Fund of China (91022033), and Postdoctoral Innovation Foundations of Shandong Province (201203051).

■ REFERENCES

(1) Lin, Z. Z.; Jiang, F. L.; Chen, L.; Yue, C. Y.; Yuan, D. Q.; Lan, A. J.; Hong, M. C. *Cryst. Growth Des.* **2007**, *7*, 1712.
(2) Wan, Y.; Zhao, D. Y. *Chem. Rev.* **2007**, *107*, 2822.
(3) Kim, E.; Son, D.; Kim, T. G.; Cho, J.; Park, B.; Ryu, K. S.; Chang, S. H. *Angew. Chem., Int. Ed.* **2004**, *43*, 5987.
(4) Xiong, S. L.; Yuan, C. Z.; Zhang, X. G.; Xi, B. J.; Qian, Y. T. *Chem.—Eur. J.* **2009**, *15*, 5320.
(5) Poizot, P.; Laruelle, S.; Grugeon, S.; Dupont, L.; Tarascon, J. M. *Nature* **2000**, *407*, 496.
(6) Kang, Y. M.; Song, M. S.; Kim, J. H.; Kim, H. S.; Park, M. S.; Lee, J. Y.; Liu, H. K.; Dou, S. X. *Electrochim. Acta* **2005**, *50*, 3667.
(7) Li, W. Y.; Xu, L. N.; Chen, J. *Adv. Funct. Mater.* **2005**, *15*, 851.
(8) Li, J. F.; Xi, B. J.; Zhu, Y. C.; Li, Q. W.; Yan, Y.; Qian, Y. T. *J. Alloys & Compds* **2011**, *509*, 9542.
(9) Alcántara, R.; Jaraba, M.; Lavela, P.; Tirado, J. L. *Chem. Mater.* **2002**, *14*, 2847.
(10) Ai, C. C.; Yin, M. C.; Wang, C. W.; Sun, J. *J. Mater. Sci.* **2004**, *39*, 1077.
(11) Sharma, Y.; Sharma, N.; Rao, G. V. S.; Chowdari, B. V. R. *J. Power Sources* **2007**, *173*, 495.
(12) Lavala, P.; Tirado, J. L.; Vidal-Abarca, T. *Electrochim. Acta* **2007**, *52*, 7986. Li, J. F.; Xiong, S. L.; Li, X. W.; Qian, Y. T. *Nanoscale* **2013**, DOI: 10.1039/C2NR33576J.
(13) Cui, B.; Lin, H.; Li, J. B.; Li, X.; Yang, J.; Tao, J. *Adv. Funct. Mater.* **2008**, *18*, 1440.
(14) Wei, T. Y.; Chen, C. H.; Chien, H. C.; Lu, S. Y.; Hu, C. C. *Adv. Mater.* **2010**, *22*, 347.
(15) Wang, X.; Han, X. D.; Lim, M. F.; Singh, N.; Gan, C. L.; Jan, M.; Lee, P. S. *J. Phys. Chem. C* **2012**, *116*, 12448.
(16) Wang, H. L.; Gao, Q. M.; Jiang, L. *Small* **2011**, *7*, 2454.
(17) Jiang, H.; Ma, J.; Li, C. Z. *Chem. Commun.* **2012**, *48*, 4465.
(18) Zhang, G. Q.; Wu, H. B.; Hoster, H. E.; Chan-Park, M. B.; Lou, X. W. *Energy Environ. Sci.* **2012**, *5*, 9453.
(19) Yuan, C. Z.; Yang, L.; Hou, L.; Shen, L. F.; Zhang, X. G.; Lou, X. W. *Energy Environ. Sci.* **2012**, *5*, 7883.
(20) Bruce, P. G.; Scrosati, B.; Tarascon, J. M. *Angew. Chem., Int. Ed.* **2008**, *47*, 2930.
(21) Fang, X.; Yu, X.; Liao, S.; Shi, Y.; Hu, Y. S.; Wang, Z.; Stucky, G. D.; Chen, L. *Microporous Mesoporous Mater.* **2012**, *151*, 418.
(22) Lu, A. H.; Schuth, F. *Adv. Mater.* **2006**, *18*, 1793.
(23) Rumplecker, A.; Kleitz, F.; Salabas, E. L.; Schuth, F. *Chem. Mater.* **2007**, *19*, 485.
(24) Yang, P.; Zhao, D.; Margolese, D. I.; Chmelka, B. F.; Stucky, G. D. *Chem. Mater.* **1999**, *11*, 2813.
(25) Fan, J.; Boettcher, S. W.; Stucky, G. D. *Chem. Mater.* **2006**, *18*, 6391.
(26) Rietveld, H. M. *J. Appl. Crystallogr.* **1969**, *2*, 65.
(27) Larson, A. C.; Von Dreele, R. B. *Los Alamos National Laboratory Report LAUR 86-748*; Los Alamos National Laboratory: Los Alamos, NM, 2004.
(28) Knop, O.; Reid, K. I. G.; Sutarno; Nakagawa, Y. *Can. J. Chem.* **1968**, *46*, 3463.
(29) Marco, J. F.; Gancedo, J. R.; Gracia, M.; Gautier, J. L.; Ríos, E. I.; Palmer, H. M.; Greaves, C.; Berry, F. J. *J. Mater. Chem.* **2001**, *11*, 3087.
(30) Wu, Y. Q.; Chen, X. Y.; Ji, P. T.; Zhou, Q. Q. *Electrochim. Acta* **2011**, *56*, 7517.
(31) Sing, K. S. W.; Everett, D. H.; Haul, R. A. W.; Moscou, L.; Pierotti, R. A.; Rouquerol, J.; Siemieniewska, T. *Pure & App. Chem.* **1985**, *57*, 603.
(32) Thissen, A.; Ensling, D.; Fernandez-Madrigal, F. J.; Jaegermann, W.; Alcantara, R.; Lavela, P.; Tirado, J. L. *Chem. Mater.* **2005**, *17*, 5202.

(33) Kim, J. G.; Pugmire, D. L.; Battaglia, D.; Langell, M. A. *Appl. Surf. Sci.* **2000**, *165*, 70.
(34) Marco, J. F.; Gancedo, J. R.; Gracia, M.; Gautier, J. L.; Ríos, E. I.; Berry, F. J. *J. Solid State Chem.* **2000**, *153*, 74.
(35) Choudhury, T.; Saied, S. O.; Sullivan, J. L.; Abbot, A. M. *J. Phys. D: Appl. Phys.* **1989**, *22*, 1185.
(36) Roginskaya, Y. E.; Morozova, O. V.; Lubnin, E. N.; Ulitina, Y. E.; Lopukhova, G. V.; Trasatti, S. *Langmuir* **1997**, *13*, 4621.
(37) Zhong, J. H.; Wang, A. L.; Li, G. R.; Wang, J. W.; Ou, Y. N.; Tong, Y. X. *J. Mater. Chem.* **2012**, *22*, 5656.
(38) Qiu, D. F.; Xu, Z. J.; Zheng, M. B.; Zhao, B.; Pan, L. J.; Pu, L.; Shi, Y. *J Solid State Electrochem.* **2012**, *16*, 1889.
(39) Xiong, S. L.; Chen, J. S.; Lou, X. W.; Zeng, H. C. *Adv. Funct. Mater.* **2012**, *22*, 861.
(40) Munichandraiah, N.; Scanlon, L. G.; Marsh, R. A. *J . Power Sources* **1998**, *72*, 203.
(41) Laruelle, S.; Grugeon, S.; Poizot, P.; Dolle, M.; Dupont, L.; Tarascon, J. M. *J. Electrochem. Soc.* **2002**, *149*, A627.
(42) Balaya, P.; Li, H.; Kienle, L.; Maier, J. *Adv. Funct. Mater.* **2003**, *13*, 621.
(43) Xing, Z.; Ju, Z. C.; Yang, J.; Xu, H. Y.; Qian, Y. T. *Nano Res.* **2012**, *5*, 477.
(44) Li, J. F.; Xiong, S. L.; Li, X. W.; Qian, Y. T. *J. Mater. Chem.* **2012**, *22*, 23254.
(45) Shaju, K. M.; Jiao, F.; Debart, A.; Bruce, P. G. *Phys. Chem. Chem. Phys.* **2007**, *9*, 1837.
(46) Jiang, J.; Li, Y. Y.; Liu, J. P.; Huang, X. T.; Yuan, C. Z.; Lou, X. W. *Adv. Mater.* **2012**, *24*, 5166.